The Indian Ocean SST dipole simulated in a coupled general circulation model

Satoshi Iizuka [1], Tomonori Matsuura

National Research Institute for Earth Science and Disaster Prevention, Tsukuba, Japan.

Toshio Yamagata [2]

Institute for Global Change Research, Frontier Research System for Global Change, Tokyo, Japan.

Abstract. We are successful in simulating the recently discovered ocean-atmosphere coupled phenomenon called the Indian Ocean Dipole for the first time, using a coupled general circulation model without flux correction. During the analyzed 50 years of model integration, the anomalous climate events have appeared 8 times over the Indian Ocean (IO). They are characterized by the cooling of the sea surface temperature (SST) in the southeastern tropical IO and the warming of the SST in the western tropical IO, associated with the anomalous easterly winds along the equator. The spatial pattern of the anomalous SST shows an east-west dipole mode (DM) structure that is similar to the recent reports. The simulated DM events are independent of the El Niño simulated in the same model. The heat budget analysis shows that the tropical air-sea interaction, which is strongly influenced by ocean dynamics, is crucial in generating the model DM events.

1. Introduction

The El Niño-Southern Oscillation (ENSO) is the most prominent interannual climate variability in the world climate. It is well known that the El Niño is associated with devastating droughts over the western tropical Pacific (called Tuarang in Indonesia), torrential floods around the eastern tropical Pacific rim, and unusual weather patterns over various parts of the world [e.g. *Philander,* 1990]. However, *Saji et al.* [1999] have recently pointed out that the Indian Ocean (IO) gives birth to another unique coupled ocean-atmosphere mode which may induce unusual rainfall in the surrounding area including the tropical East Africa. They have called the new climate signal the "Dipole Mode (DM)" based on the sea surface temperature (SST) and corresponding wind anomalies over the tropical IO. *Webster et al.* [1999] and *Yu and Rienecker* [1999] also reported the DM event occurred during 1997-98. According to *Saji et al.* [1999], the DM event actually occurred in 1961, 1967, 1972, 1982, 1994, and 1997.

The DM structure is characterized by the cold SST anomaly (SSTA) in the southeastern tropical IO (SETIO) and the warm SSTA in the western tropical IO (WTIO) [*Vinayachandran et al.,* 1999; *Behera et al.,* 1999; *Saji et al.,* 1999; *Webster et al.,* 1999; *Yu and Rienecker,* 1999; *Murtugudde et al.,* 2000]. In response to the SSTA, atmospheric convection over the eastern (western) tropical IO is suppressed (enhanced), and the easterly wind anomaly over the central IO is intensified. Tuarang (abnormally dry season) in Indonesia may be related to the DM event in the IO as well as the El Niño in the Pacific. The anomalous wind related to the DM event causes a shoaling (deepening) of the thermocline in the eastern (western) equatorial IO. This results in the cooling (warming) of SSTs in the east (west) by increasing (decreasing) entrainment from below the thermocline. Thus, the positive feedback due to the air-sea interaction is crucial in the variability related to the DM event. This situation is quite similar to the El Niño in the tropical Pacific.

In the present article, we first describe the DM events simulated using a high-resolution coupled ocean-atmosphere general circulation model (CGCM). Then we analyze the heat budget to clarify the manner in which the SSTAs are formed. The CGCM is composed of the T106 AGCM developed by the JMA (GSM8911) and the GFDL OGCM (MOM2) [see *Matsuura et al.,* 1999 for details]. We note that the model climatology (particularly, SST and wind fields) over the IO is in good agreement with observations. The simulated precipitation, however, is less near the Philippines and more over the eastern Tibetan Plateau during the boreal summer than the actual observed precipitation (Fig. 1).

2. Model Dipole Mode

Figure 2 shows the model DM index that is defined as the difference in SSTA between the WTIO (50°E-70°E, 10°S-10°N) and the SETIO (90°E-110°E, 10°S-Equator), as in *Saji et al.* [1999]. The extreme DM event occurs in model years 15, 16, 30, 41, 46, 47, 49, and 56 if we define the event when the DM index shows variations one and a half times larger than the standard deviation. The two area-averaged SSTAs tend to fluctuate out of phase with a phase lag of a few months (see Fig. 3). The highest correlation is -0.4 when the SSTA in the SETIO leads that in the WTIO by four months; this is significant at the 95 % confidence level. As in the observational data analysis [*Saji et al.,* 1999], the model DM index is strongly related to the zonal surface winds over the tropical IO (70°E-90°E, 5°S-5°N) with a correlation of -0.65. The model DM events are not related to the SSTA in the Niño3 region (150°W-90°W, 5°S-5°N); the correlation between those two indices is only 0.06. In contrast to the positive DM events, the negative DM events (warm SSTA

[1]also at IGCR,FRSGC

[2]also at Department of Earth and Planetary Science, Graduate School of Science, The University of Tokyo, Japan.

Paper number 1999GL000000.
0094-8276/00/1999GL000000$05.00

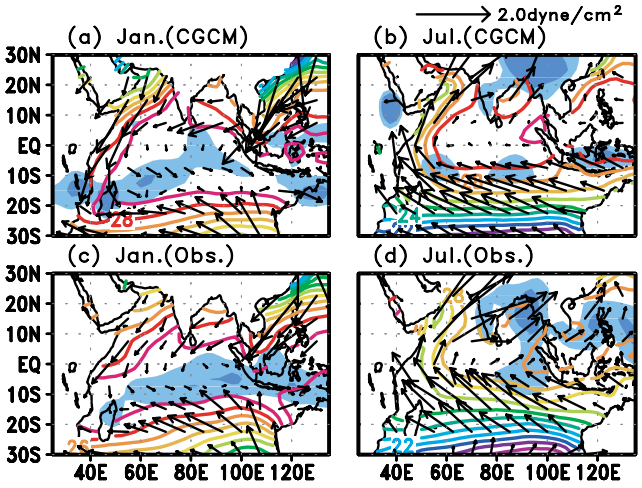

Figure 1. Simulated climatological SST, wind stress, and precipitation in January (a) and in July (b). (c) Same as in (a) but for observations. (d) Same as in (b) but for observations. Contour interval is 1°C. Light shading indicates precipitation more than 8 mm day^{-1}. The area for precipitation more than 12 mm day^{-1} is highlighted by dark shading. The observed conterparts are derived from Reynolds and Smith (1994)'s SST, Xie and Arkin (1996)'s rainfall, and Hellerman and Rosenstein (1983)'s wind stress data sets, respectively.

over the SETIO and cold SSTA over WTIO, associated with the westerly wind anomalies) also appear interannually as in the observations. However we have not described the negative DM events in the present article because the situation is similar to that of the positive DM events except for the sign.

In order to describe the evolution of the model DM events in detail, we have conducted a composite analysis of the model SST and wind stress anomalies for the 8 events (Fig. 3). Accompanied by the southeasterly wind anomaly, the cold SSTA first appears along the coast of Java in June (not shown). In July, the cold SSTA extends to the west along the Sumatra coast, and the easterly wind anomaly appears over the tropical IO (Fig. 3a). In September, the zonal wind anomaly over the tropical IO further intensifies, while the southeasterly wind anomaly along the Sumatra weakens (Fig. 3b). In response to the SST changes, convection is suppressed (enhanced) over the eastern (western) tropical IO. This results in the anomalous Walker Circulation (WC) over the tropical IO, as seen in the convergence (divergence) field of wind at 200 hPa over the eastern (western) tropical IO (Fig. 4a). This anomalous WC associated with the easterly wind anomaly in the lower troposphere leads to decreased (increased) precipitation over the eastern (western) tropical IO (Fig. 4b). The easterly wind anomaly generates the anomalous westward current over the equatorial IO; it also causes the shallower (deeper) thermocline in the eastern (western) equatorial IO (Fig. 4c). This leads to the decrease (increase) of SST in the eastern (western) tropical IO. While the SSTA in the SETIO weakens after November (Fig. 3c), the SSTA in the WTIO continues to increase and reaches its peak in the following January (Fig. 3d).

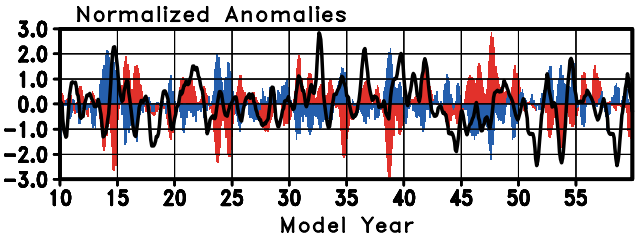

Figure 2. Time series of the model DM index (red), equatorial zonal surface wind over the IO (blue), and SSTA in Niño3 (black). All time series are computed using a 5-month running mean filter and normalized by the respective standard deviations (σ_{DMI} = 0.45°C, σ_{Ueq} = 0.86 m s^{-1}, $\sigma_{Niño3}$ = 0.47°C).

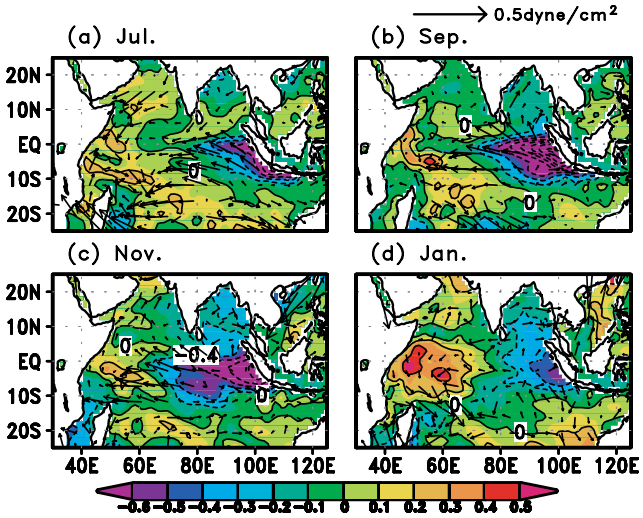

Figure 3. Composite maps of SST and wind stress anomalies for July (a), September (b), November (c), and January (d). Contour interval is 0.2°C.

Another interesting feature of the DM events is that the positive anomalies of the sea level height along 10°S intensify and expand westward (Fig. 4c). Actually, such sea level height anomalies are observed during 1997-98 DM event [*Webster et al.,* 1999]. The above features of the simulated DM events are quite similar to the picture based on the data analysis, although the model fails to capture the biennial tendency of the DM events [cf. *Saji et al.,* 1999].

3. Heat Budget

We have investigated the evolution of the simulated SST changes in Area A (90°E-110°E, 10°S-Equator) and Area B (30°E-70°E, 5°S-5°N) during the DM events. Those areas are chosen to cover two centers of the model SST dipole. We first calculate a seasonal climatology of heat budget for the model 50 years in two boxes (Box A and B) surrounded by the Area A and B down to the depth of 60 m and then a composite for the 8 DM events (Fig. 5). The difference of those two is used to depict the evolution of the anomalous field during the DM events.

During the DM events, the negative anomalous tendency of the heat budget in Box A from late May to August is due to the vertical and horizontal divergence of heat transport (Fig. 5b). The vertical divergence indicates that cold water is brought into the surface as the thermocline shallows in response to the southeasterly wind anomaly over the IO. The horizontal divergence corresponds to the advection of cold surface water induced by the anomalous westward current

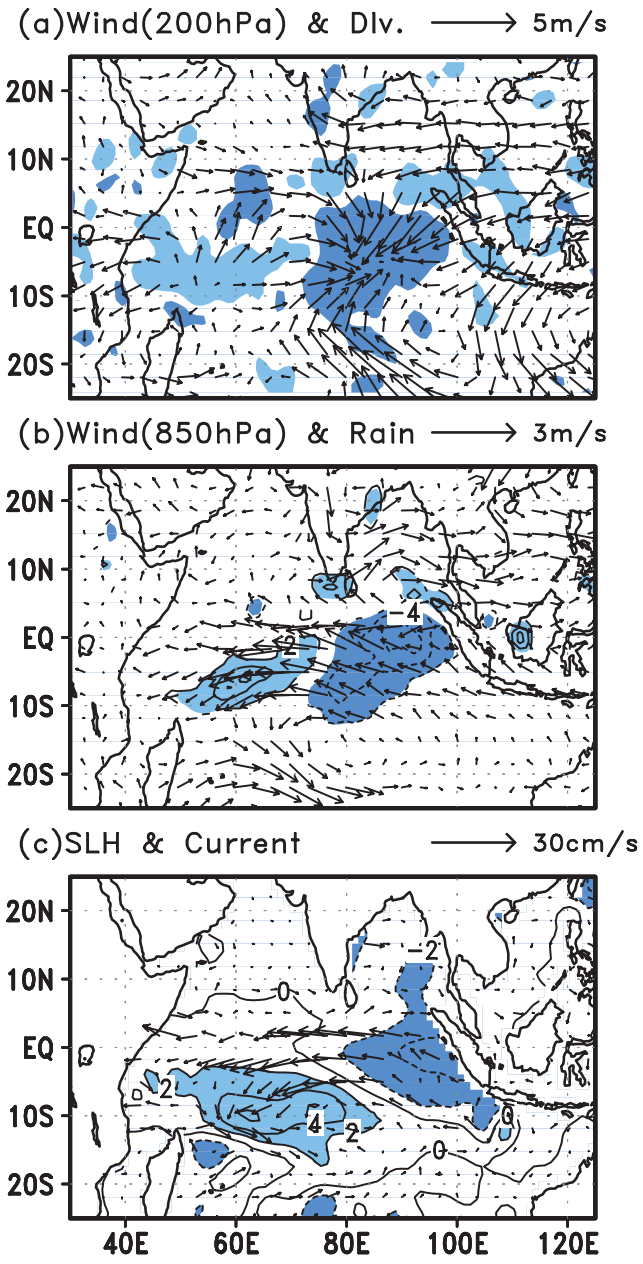

Figure 4. (a) Composite map of model wind and divergence anomalies at 200 hPa in September during the DM events. Light shading indicates divergence more than 1x10^{-6} s^{-1}; dark shading indicates convergence less than -1x10^{-6} s^{-1}. (b) Same as in (a) except for the model wind at 850 hPa and precipitation anomalies. Contour interval is 2 mm day^{-1} and zero contour is omitted. Light shading indicates precipitation anomalies more than +2 mm day^{-1}; dark shading indicates less than -2 mm day^{-1}. (c) Same as in (a) except for sea level height and surface current anomalies. Contour interval is 2 cm. Light shading represents sea level height anomalies more than +2 cm; dark shading is for the area less than -2 cm.

excited by the southeasterly wind anomaly. The evaporative cooling effect does not contribute toward lowering the SST in Box A except in June. This is mainly because the lowered SST reduces the evaporation in our CGCM.

In September, the negative SSTA in Area A reaches its peak (Fig. 5a). At the same time, the time-tendency of heat content in Box A changes sign and becomes positive. This warming is partially due to the increased insolation resulting from the seasonal march, which is accelerated by decreased cloudiness in response to the cold SSTA (not shown). In regard to the DM phase locked to the annual cycle, we note that the weakening of wind speed due to the reversal of the monsoonal wind is responsible for the basic seasonal warming. The warm water accumulation due to the impinging fall Wyrtki jet, which is excited by the zonal wind in the central IO during the monsoon transition season [see *Clark and Liu,* 1993; *Yamagata et al.,* 1996], may also contribute toward terminating the seasonal cooling in the eastern IO.

The heat content in Box B starts increasing in late October, which is mainly due to the vertical convergence of heat transport (Fig. 5d). Since the thermocline in the WTIO deepens in response to the anomalous easterly wind, the reduction of cold water entrainment from the subsurface layer leads to warmer than normal SST in the region. The warm SSTA in the WTIO reaches its peak in January (Fig. 5c). At least in our CGCM, the surface heat flux anomaly does not contribute toward increasing the SST in Box B during the DM events even though it contributes toward warming of SST outside Box B as in *Yu and Rienecker* [1999]. We note here that the model SST warming in Box B delays by three or four months in comparison with observational evidence [*Saji et al.,* 1999]. Model biases in ocean mixed-layer physics as well as in surface fluxes may be responsible for this discrepancy through excessive westward extension of the cold SSTA.

4. Remarks

Using a high-resolution CGCM, we have succeeded in simulating the major characteristics of the DM events over

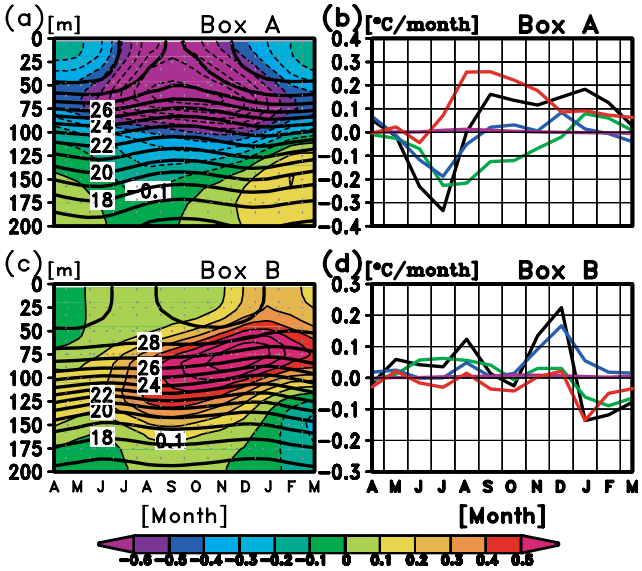

Figure 5. ((a) Seasonal cycle of temperature anomalies during the DM events in Box A. Contour interval is 0.1°C. Climatological temperature are also shown by thick lines. Contour interval is 1°C. (b) Heat budget anomaly in the Box A during the DM events. The time-tendency of heat content in the upper 60 m (black) is composed of the horizontal (green) and vertical (blue) convergence of heat transport, the surface heat flux (red), and diffusive process (purple), respectively. (c) Same as in (a) except for Box B. (d) Same as in (b) except for Box B.

the tropical IO. The temporal evolution and spatial patterns of the simulated DM events are mostly in good agreement with observational evidence [*Saji et al.,* 1999]. The simulated DM events are clearly independent of the model El Niño events in the present CGCM. The observational analysis also suggests that the DM event may occur independently of the ENSO as a unique air-sea coupled phenomenon over the tropical IO [*Saji et al.,* 1999; *Webster et al.,* 1999]. The heat budget analysis demonstrates that an air-sea interaction, strongly influenced by the ocean dynamics, is essential in the evolution of the model DM events.

We note that seasonal dependence is a prominent feature of the DM events. Normally, the SST in the SETIO is cool from boreal summer to fall. This situation is due to the southeasterly monsoon winds which blow along the coast of Indonesia from June through October, while the direction of winds is reversed during the boreal winter. The anomalous cooling of the SST in the SETIO during the DM events occurs only during the boreal summer monsoon season; the unusual intensification of southeasterly winds along the coast of Indonesia is a direct cause triggering the DM events.

It is certainly necessary to enhance our understanding of the newly catalogued air-sea coupled phenomenon over the IO from both observational and modeling perspectives. Here we have demonstrated that a CGCM is one of the powerful tools in this direction.

Acknowledgments. The authors would like to thank Drs. S. K. Behera, G. Ilahude, R. Kawamura, N. H. Saji, and C. Shaji for helpful discussions and suggestions. The work was supported by the Japan Science and Technology Agency (JSTA) through NIED as well as by FRSGC of JAMSTEC/NASDA under JSTA. We acknowledge the Japan Meteorological Agency and the Geophysical Fluid Dynamics Laboratory/NOAA for the prototype codes of GCMs used in the present study. Figures are prepared using the GrADS software.

References

Behera, S. K., S. Krishnan, and T. Yamagata, Unusual Ocean-Atmosphere conditions in the tropical Indian Ocean during 1994. *Geophys. Res. Lett., 26*, 3001-3004, 1999.

Clark, A. J., and X. Liu, Observations and dynamics of semiannual and annual sea levels near the eastern equatorial Indian Ocean boundary. *J. Phys. Oceanogr., 23*, 386-399, 1993.

Hellerman, S., and M. Rosensein, Normal monthly wind stress over the world's ocean with error estimates. *J. Phys. Oceanogr., 13*, 1093-1104, 1983.

Matsuura, T., M. Yumoto, S. Iizuka, and R. Kawamura, Typhoon and ENSO simulation using a high-resolution coupled GCM. *Geophys. Res. Lett., 26*, 1755-1758, 1999.

Murtugudde, R., J. P. McCreary, and A. J. Busalacchi, Oceanic processes associated with anomalous events in the Indian Ocean with relevance to 1997-1998. *J. Geophy. Res., 105*, 3295-3306, 2000.

Philander, S. G. H., El Nino, La Nina and the Southern Oscillation. Academic Press, New York, 289 pp, 1990.

Reynolds, R. W., and T. M. Smith, A high resolution global sea surface temperature climatology. *J. Climate, 8*, 1572-1583, 1995.

Saji, N. H., B. N. Goswami, P. N. Vinayachandran, and T. Yamagata, A dipole mode in the tropical Indian Ocean. *Nature, 401*, 360-363, 1999.

Vinayachandran. P. N., N. H. Saji, and T. Yamagata, Response of the equatorial Indian Ocean to an unusual wind event during 1994. *Geophys. Res. Lett., 26*, 1613-1615, 1999.

Webster, P. J., A. M. Moore, J. P. Loschnigg, and R. R. Leben, Coupled oceanic-atmospheric dynamics in the Indian Ocean during 1997-98. *Nature, 401*, 356-360, 1999.

Xie, P., and P. A. Arkin, Analyses of global monthly precipitation using gauge observations, satellite estimates and numerical model predictions. *J. Climate, 9*, 840-858, 1996.

Yamagata, T., K. Mizuno, and Y. Masumoto, Seasonal variations in the equatorial Indian Ocean and their impact on the Lombok throughflow. *J. Geophys. Res.,101*, 12,465-12,473, 1996.

Yu, L, and M. M. Rienecker, Mechanisms for the Indian Ocean warming during the 1997-98 El Nino. *Geophys. Res. Lett., 26*, 735-738, 1999.

S. Iizuka, T. Matsuura, National Research Institute for Earth Science and Disaster Prevention, Tennodai 3-1, Tsukuba, Ibaraki, 305-0006, Japan.(e-mail: iizuka@ess.bosai.go.jp; matsuura@ess.bosai.go.jp)

T. Yamagata, Institute for Global Change Research, Frontier Research System for Global Change, SEAVANS North 7F, 1-2-1, Shibaura, Minato-ku, Tokyo, 105-6791, Japan.(e-mail: yamagata@eps.s.u-tokyo.ac.jp)

(Received February 3, 2000; accepted July 17, 2000)